

Valley depolarization due to inter- and intra-valley electron-hole exchange interactions in monolayer MoS₂

T. Yu and M. W. Wu*

*Hefei National Laboratory for Physical Sciences at Microscale and Department of Physics,
University of Science and Technology of China, Hefei, Anhui, 230026, China*
(Dated: August 28, 2018)

We investigate the valley depolarization due to the electron-hole exchange interaction in monolayer MoS₂. Both the long- and short-range parts of the intra- and inter-valley electron-hole exchange interactions are calculated. We find that both the long- and short-range exchange interactions can cause the inter- and intra-valley bright exciton transitions. With the intra-valley bright exciton transition channel nearly forbidden due to the large splitting of the valence bands, the inter-valley channel due to the exchange interaction can cause the valley depolarization efficiently by the Maialle-Silva-Sham mechanism [Phys. Rev. B **47**, 15776 (1993)]. With only the long-range exchange interaction, the calculations show good agreement with the recent valley polarization experiments, including the time-resolved valley polarization measurement, the pump-probe experiment and the steady-state PL polarization measurement. We further show that for the A-exciton with large (small) center-of-mass momentum, the long-range exchange interaction can cause the *fast* (*slow*) inter-valley exciton transition.

PACS numbers: 71.70.Gm, 71.35.-y, 78.67.-n

I. INTRODUCTION

Monolayer MoS₂ has attracted intense interest due to its remarkable electrical and optical properties from its unique energy band structure (shown in Fig. 1) very recently.¹⁻¹⁷ Unlike its bulk form, monolayer MoS₂ has direct gaps at the inequivalent K and K' points of the hexagonal Brillouin Zone,⁸⁻¹³ which have been confirmed in the photoluminescence (PL) experiments.⁴⁻⁷ In addition, due to the space inversion asymmetry and the strong spin-orbit coupling originated from the *d*-orbitals of the heavy metal atoms, the valence bands are split by about 160 meV.^{6,9,11,14-17} Therefore, it shows two excitonic transitions A (≈ 1.9 eV) and B (≈ 2.1 eV) from the K or K' point in the light absorption.^{5,7,18-21} Moreover, the chiral optical valley selection rule in this system leads to the selective excitation of carriers in only one of these valleys depending on the helicity of circularly polarized light, with σ_+ or σ_- light being directly associated with the K or K' valley.⁴⁻⁶ Accordingly, the spin polarization can be realized due to the splitting of the valence bands.⁴⁻⁷ Therefore, monolayer MoS₂ provides an ideal platform to study the semiconductor valley physics (valleytronics).

It has been theoretically predicted that high valley polarization up to 100% can be realized in monolayer MoS₂.^{5-8,18-21} However, recent valley polarization experiments in monolayer MoS₂ with A-exciton pumped, including the time-resolved valley polarization measurement,²¹ the pump-probe experiment^{22,23} and the steady-state PL polarization measurement,^{5-8,18-20} suggest that there exists fast valley depolarization. For the time-resolved valley polarization measurement, the observation of the excitonic signal in the K' valley is immediate after the A-exciton pumped in the K valley and a

finite valley polarization (about 50% at 4 K) is measured during the A-exciton lifetime.²¹ For the pump-probe experiment, it shows that there also exists fast inter-valley exciton transition and finite residue valley polarization which lasts for tens of picoseconds.^{22,23} In the steady-state measurements of the PL polarization, a wide range of valley polarizations from 30% to 100% are reported with the resonantly pumping energy $E \approx 1.96$ eV for the A exciton at low temperature.^{5,7,18-21} It was claimed that the valley depolarization originates from the electron/hole spin relaxation due to the D'yakonov-Perel' (DP)²⁴ and Elliott-Yafet (EY)^{25,26} mechanisms.^{5,7,18-21} Therefore, after the inter-valley scattering including the electron-phonon^{5,18,19,21} and/or short-range impurity scatterings, the spin relaxation of the electron and hole can cause the bright exciton transition between the K and K' valleys and hence the PL depolarization. However, for the DP mechanism, in the *intrinsic* situation, it cannot cause any spin relaxation because the out-of-plane component of the electron or hole spin is conserved,^{6,27-29} in the *extrinsic* situation, the flexural deformations can cause the spin relaxation of carriers but the spin relaxation time is in the order of nanoseconds.^{30,31} For the EY mechanism, the out-of-plane components of the electron or hole spin are conserved in the intrinsic situation and only the extrinsic influences can cause the spin relaxation.^{6,27-30} It is calculated that the spin relaxation time of the out-of-plane component is also in the order of nanoseconds at low temperature with low impurity density.³² Accordingly, the exciton transition time due to the DP and EY mechanisms is much longer than its lifetime, which is in the order of picoseconds,^{21,33} and hence the DP and EY mechanisms cannot cause the PL depolarization effectively.

In this paper, we show that the electron-hole (e-h)

exchange interaction can cause the valley depolarization efficiently due to the Maialle-Silva-Sham (MSS) mechanism^{34,35} based on the kinetic spin Bloch equations (KSBEs).^{36,37} We show that both the long-range (L-R) and short-range (S-R) parts of the exchange interactions can cause the inter- and intra-valley bright exciton transitions. However, the intra-valley bright exciton transition channel is nearly forbidden due to the large splitting of the valence bands and only the inter-valley exchange interaction can cause the valley depolarization efficiently. This inter-valley bright exciton transition process is schematically shown in Fig. 1, in which electrons in the conduction band of the K valley and valence band in the K' valley are scattered to the valence band in the K valley and conduction band in the K' valley, respectively. This process can also be treated as the result of virtual recombination of a bright exciton in the K valley and generation in the K' valley, or vice versa. We further show that for the A-exciton with large center-of-mass momentum, the L-R exchange interaction can cause the *fast* inter-valley exciton transition. This explains the fast emergence of the excitonic signal in the K' valley with the A-exciton pumped in K valley in the experiments.²¹⁻²³ However, for the A-exciton with small center-of-mass momentum, the inter-valley exciton transition is relatively *slow*, which leads to the existence of the residue valley polarization which lasting for tens of picoseconds in the experiments.^{22,23}

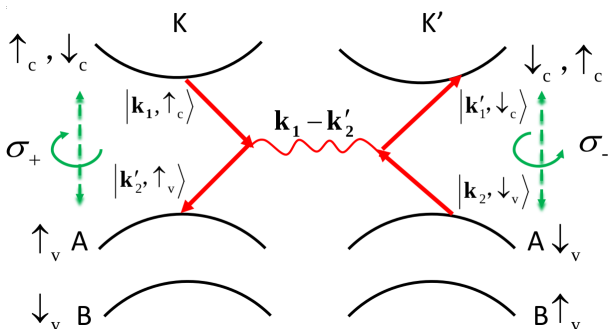


FIG. 1: (Color online) Schematic diagram of the bright exciton transition channel between the K and K' valleys. The Feynman diagram shows that due to the short-range exchange interaction, the electrons in the states $|\mathbf{k}_1, \uparrow_c, K\rangle$ and $|\mathbf{k}_2, \downarrow_v, K'\rangle$ are scattered to the states $|\mathbf{k}_2, \uparrow_v, K\rangle$ and $|\mathbf{k}_1, \downarrow_c, K'\rangle$, respectively. Consequently, the inter-valley bright exciton transition is realized by the virtual recombination of a bright exciton in the K valley and then generation in the K' valley or vice versa.

This paper is organized as follows. In Sec. II, we set up the model and lay out the formalism. In Sec. II A, we derive the L-R and S-R parts of the exciton exchange interaction Hamiltonian and show that both the L-R and S-R exchange interactions can cause the inter-valley exciton transition. In Sec. II B, we present the KSBEs and compare the theoretical results with the experimental ones. We conclude and discuss in Sec. III.

II. MODEL AND FORMALISM

A. E-h exchange interaction

In this work, we study the e-h exchange interaction for the direct excitons in monolayer MoS₂ based on the lowest four band $\mathbf{k}\cdot\mathbf{p}$ Hamiltonian for the K (K') valley:^{6,28,29}

$$\hat{H} = at(\tau k_x \hat{\sigma}_x + k_y \hat{\sigma}_y) + \Delta \hat{\sigma}_z / 2 - \lambda \tau (\hat{\sigma}_z - 1) \hat{s}_z / 2. \quad (1)$$

Here, a is the lattice constant, t represents the effective hopping integral; τ is the valley index for K ($\tau = 1$) and K' ($\tau = -1$) valleys; $\hat{\sigma}$ stand for the Pauli matrices for the two basis functions [c (v) indicates conduction (valence) band]

$$|\phi_c\rangle = |d_{z^2}\rangle, \quad |\phi_v^\tau\rangle = \frac{1}{\sqrt{2}}(|d_{x^2-y^2}\rangle + i\tau|d_{xy}\rangle); \quad (2)$$

Δ is the energy gap; 2λ denotes the spin splitting of the valence bands and \hat{s}_z is the Pauli matrix for spin.⁶ Using above Hamiltonian Eq. (1), the effective Hamiltonian for the exciton envelop function in the coordinate space are derived following the previous works within the framework of the effective-mass approximation [refer to Eq. (A4)],^{34,38,39} shown in Appendix A. Based on this effective Hamiltonian Eq. (A2), by treating MoS₂ as ideal two-dimensional (2D) material,⁴⁰ the basis functions for the direct excitons can be expressed in terms of the exciton ground state

$$|\mu_e, \nu_h, \mathbf{P}, \mathbf{K}\rangle = \Psi_{\mathbf{K}}^{\mu_e}(\mathbf{r}_e) \tilde{\Psi}_{\mathbf{K}}^{\nu_h}(\mathbf{r}_h) \phi_{1s}^{2D}(\boldsymbol{\rho}) e^{i\mathbf{P}\cdot\mathbf{R}} / \sqrt{S} \quad (3)$$

for the K valley and

$$|\mu'_e, \nu'_h, \mathbf{P}', \mathbf{K}'\rangle = \Psi_{\mathbf{K}'}^{\mu'_e}(\mathbf{r}_e) \tilde{\Psi}_{\mathbf{K}'}^{\nu'_h}(\mathbf{r}_h) \phi_{1s}^{2D}(\boldsymbol{\rho}) e^{i\mathbf{P}'\cdot\mathbf{R}} / \sqrt{S} \quad (4)$$

for the K' valley. In Eqs. (3) and (4), $\Psi_{\mathbf{K}(\mathbf{K}')}^{\mu_e(\mu'_e)}(\mathbf{r}_e)$ and $\tilde{\Psi}_{\mathbf{K}(\mathbf{K}')}^{\nu_h(\nu'_h)}(\mathbf{r}_h)$ are the electron and hole Bloch wave functions with μ_e (μ'_e) and ν_h (ν'_h) denoting the electron spin in the conduction bands and hole spin in the valence bands (note $\nu_h = -\nu_e$ with ν_e being the electron spin in the valence bands), respectively; $\phi_{1s}^{2D}(\boldsymbol{\rho}) = \sqrt{8/\pi a_B^2} \exp(-2\rho/a_B)$ is the 2D hydrogenic exciton ground-state wave function with $\boldsymbol{\rho} = \mathbf{r}_e - \mathbf{r}_h$ standing for the relative coordinate of the electron and hole, and a_B is the exciton radius; the last factor represents the center-of-mass motion of the exciton with S , \mathbf{P} (\mathbf{P}') and \mathbf{R} representing the area of the 2D plane of MoS₂, the center-of-mass wavevector of the electron-hole pair and its center-of-mass position, respectively.

The exchange interaction is divided into the L-R and S-R parts. Their matrix elements between two exciton ground states are further derived based on the exciton Hamiltonian in Appendix A by expanding the exciton envelop function using the exciton ground states,^{34,38,39} which are shown as follows.

1. L-R part

For the L-R part of the exchange interaction, there exist matrix elements for the excitons in a single valley or between \mathbf{K} and \mathbf{K}' valleys.^{34,38} The matrix elements between two exciton ground states $|m, n, \mathbf{P}, \mathbf{k}_0\rangle$ and $|m', n', \mathbf{P}', \mathbf{k}'_0\rangle$ are expressed as

$$B_{\mathbf{k}_0-\mathbf{k}'_0}^{\text{L-R}} = \frac{e^2}{2\kappa\varepsilon_0|\mathbf{P}|} \delta_{\mathbf{P},\mathbf{P}'} |\phi_{1s}^{2D}(0)|^2 Q_{\Theta n' m}^{\mathbf{k}_0-\mathbf{k}'_0}(\mathbf{P}), \quad (5)$$

with ε_0 and κ standing for the vacuum permittivity and relative dielectric constant, respectively; $\mathbf{k}_0(\mathbf{k}'_0)$ representing \mathbf{K} or \mathbf{K}' ;

$$Q_{\Theta n' m}^{\mathbf{k}_0-\mathbf{k}'_0}(\mathbf{P}) = \frac{\hbar^2}{m_0^2} [\mathbf{P} \cdot \boldsymbol{\pi}_{m'\Theta n'}(\mathbf{k}_0)] [\mathbf{P}' \cdot \boldsymbol{\pi}_{\Theta nm}(\mathbf{k}'_0)] \times \frac{1}{[E_m(\mathbf{k}_0) - E_n(\mathbf{k}_0)] [E_{m'}(\mathbf{k}'_0) - E_{n'}(\mathbf{k}'_0)]}. \quad (6)$$

Here, m_0 is the free electron mass; $\boldsymbol{\pi}_{m'\Theta n'}(\mathbf{k}_0)$ and $\boldsymbol{\pi}_{\Theta nm}(\mathbf{k}'_0)$ come from the $\mathbf{k} \cdot \mathbf{p}$ matrix elements in the Hamiltonian [Eq. (1)] with Θ being the time reversal operator (refer to Appendix A); $E_\mu(\mathbf{k})$ and $E_\nu(\mathbf{k}')$ are the edge energies of the conduction band with electron spin μ and valence band with hole spin ν .

For the intra-valley exciton exchange interaction, according to Eq. (5), with the spin bases (μ_e, ν_h) in the order $(\uparrow_e, \downarrow_h), (\downarrow_e, \downarrow_h), (\uparrow_e, \uparrow_h), (\downarrow_e, \uparrow_h)$, the L-R part of the exchange interaction between two exciton states $|m, n, \mathbf{P}, \mathbf{k}_0\rangle$ and $|m', n', \mathbf{P}', \mathbf{k}'_0\rangle$ is written as

$$H_{\mathbf{k}_0-\mathbf{k}'_0}^{\text{L-R}} = C \delta_{\mathbf{P},\mathbf{P}'} |\mathbf{P}| \begin{pmatrix} \alpha(\tau) & 0 & 0 & \beta \\ 0 & 0 & 0 & 0 \\ 0 & 0 & 0 & 0 \\ \beta & 0 & 0 & \alpha(-\tau) \end{pmatrix}. \quad (7)$$

Here, $C = e^2/(2\kappa\varepsilon_0)|\phi_{1s}^{2D}(0)|^2$ and $\tau = 1(-1)$ for $\mathbf{k}_0 = \mathbf{K}(\mathbf{K}')$. The parameters $\alpha(\tau) = a^2 t^2 / (\Delta - \tau \lambda)^2$ and $\beta = a^2 t^2 / (\Delta^2 - \lambda^2)$ for MoS_2 , WS_2 , MoSe_2 and WSe_2 are shown in Table I calculated with the material parameters taken from Ref. 6.

TABLE I: Material parameters $\alpha(\tau)$ and β for MoS_2 , WS_2 , MoSe_2 and WSe_2 with the unit being \AA^2 .

| | $\alpha(1)$ | $\alpha(-1)$ | β |
|-----------------|-------------|--------------|---------|
| MoS_2 | 4.91 | 4.10 | 4.49 |
| WS_2 | 7.73 | 4.77 | 6.07 |
| MoSe_2 | 5.09 | 3.99 | 4.51 |
| WSe_2 | 8.27 | 4.63 | 6.19 |

For the inter-valley exciton exchange interaction, the L-R part of the exchange interaction between the initial exciton state $|m, n, \mathbf{P}, \mathbf{K}\rangle$ and the final one

$|m', n', \mathbf{P}', \mathbf{K}'\rangle$ is written as

$$H_{\mathbf{K}-\mathbf{K}'}^{\text{L-R}} = -C \delta_{\mathbf{P},\mathbf{P}'} \frac{P_\pm^2}{|\mathbf{P}|} \begin{pmatrix} \beta & 0 & 0 & \alpha(1) \\ 0 & 0 & 0 & 0 \\ 0 & 0 & 0 & 0 \\ \alpha(-1) & 0 & 0 & \beta \end{pmatrix} \quad (8)$$

with $P_\pm = P_x \pm iP_y$.

From Eqs. (7) and (8), both the intra- and inter-valley L-R exchange interactions can cause the valley depolarization by the MSS mechanism.^{34,35} In the MSS mechanism, similar to the DP mechanism,²⁴ the L-R exchange interaction provides a \mathbf{P} -dependent effective magnetic field $\boldsymbol{\Omega}(\mathbf{P})$, around which the “spins” of the exciton with different center-of-mass momentums process with different frequencies, i.e., the inhomogeneous broadening.^{36,37} This inhomogeneous broadening can cause a free-induction-decay due to the destructive interference without the exciton scattering. When there exists exciton scattering with the momentum relaxation time denoted by τ_P^* , the system can be divided into the weak and strong scattering regimes: in the weak scattering regime with $\langle |\boldsymbol{\Omega}(\mathbf{P})| \rangle \tau_P^* \gtrsim 1$, the momentum scattering opens a spin relaxation channel and the exciton “spin” relaxation time $\tau_s \propto \tau_P^*$; in the strong scattering regime with $\langle |\boldsymbol{\Omega}(\mathbf{P})| \rangle \tau_P^* \ll 1$, the momentum scattering suppresses the inhomogeneous broadening and $\tau_s^{-1} = \langle \boldsymbol{\Omega}^2(\mathbf{P}) \rangle \tau_P^*$. Here, $\langle \dots \rangle$ denotes the ensemble average.

For the intra-valley exchange interaction, from Eq. (7), when there exists a large splitting of the valence bands the intra-valley depolarization channel by the MSS mechanism is nearly forbidden due to the detuning effect.⁴¹ For the inter-valley exciton exchange interaction, from Eq. (8), there exist only matrix elements between the bright exciton states. Accordingly, it can cause the valley depolarization due to the MSS mechanism. Specifically, this inter-valley depolarization channel can be efficient between two energy-degenerate exciton states when $|\mathbf{P}| \neq 0$.

2. S-R part

We then express the S-R part of the exchange interaction, which can exist not only in a single valley, but also between two different valleys. Their matrix elements between the two exciton states $|m, n, \mathbf{P}, \mathbf{k}_0\rangle$ and $|m', n', \mathbf{P}', \mathbf{k}'_0\rangle$ are expressed as

$$B_{\mathbf{k}_0-\mathbf{k}'_0}^{\text{S-R}} = \frac{1}{S} \delta_{\mathbf{P},\mathbf{P}'} |\phi_{1s}^{2D}(0)|^2 \int [\Psi_{\mathbf{k}'_0}^{m'}(\mathbf{r}_1)]^* [\Theta \tilde{\Psi}_{\mathbf{k}_0}^n(\mathbf{r}_2)]^* \times U(\mathbf{r}_1 - \mathbf{r}_2) [\Theta \tilde{\Psi}_{\mathbf{k}'_0}^{n'}(\mathbf{r}_1)] \Psi_{\mathbf{k}_0}^m(\mathbf{r}_2) d\mathbf{r}_1 d\mathbf{r}_2. \quad (9)$$

Here, $U(\mathbf{r}_1 - \mathbf{r}_2) = e^2/(4\pi\kappa\varepsilon_0|\mathbf{r}_1 - \mathbf{r}_2|)$ is the Coulomb potential; $\mathbf{k}_0(\mathbf{k}'_0)$ represents the \mathbf{K} or \mathbf{K}' .

Accordingly, by using the conduction band and valence band wave functions Eq. (2), the S-R part of the exchange

interaction between the initial exciton state $|m, n, \mathbf{P}, \mathbf{k}_0\rangle$ and the final one $|m', n', \mathbf{P}', \mathbf{k}'_0\rangle$ is written as

$$H_{\mathbf{k}_0-\mathbf{k}'_0}^{\text{S-R}} = \Xi \delta_{\mathbf{P}, \mathbf{P}'} \begin{pmatrix} 1 & 0 & 0 & 1 \\ 0 & 0 & 0 & 0 \\ 0 & 0 & 0 & 0 \\ 1 & 0 & 0 & 1 \end{pmatrix}. \quad (10)$$

Here,

$$\Xi = \frac{1}{S} |\phi_{1s}^{2\text{D}}(0)|^2 \frac{e^2}{4\pi\kappa\epsilon_0} \frac{1}{2\pi} \int \left\{ |A(\mathbf{q})|^2 + |B(\mathbf{q})|^2 + i[A^*(\mathbf{q})B(\mathbf{q}) - A(\mathbf{q})B^*(\mathbf{q})] \right\} \frac{d\mathbf{q}}{2q}, \quad (11)$$

in which

$$A(\mathbf{q}) = \langle d_{z^2} | e^{i\mathbf{q}\cdot\mathbf{r}} | d_{x^2-y^2} \rangle, \quad B(\mathbf{q}) = \langle d_{z^2} | e^{i\mathbf{q}\cdot\mathbf{r}} | d_{xy} \rangle. \quad (12)$$

From Eq. (10), for both the intra- and inter-valley exchange interactions, there exist only matrix elements between the bright exciton states, and hence both the intra- and inter-valley S-R exchange interactions can only cause the bright exciton transition. By considering the large splitting of the valence bands, the intra-valley depolarization channel due to the intra-valley S-R exchange interaction is nearly forbidden, and hence only the inter-valley S-R exchange interaction can contribute to the valley depolarization.

B. Valley depolarization due to the inter-valley e-h exchange interaction

1. Model and KSBEs

From Sec. II A, we conclude that only the inter-valley e-h exchange interaction can cause the valley depolarization efficiently. For the A-exciton pumped, the exchange interaction includes the L-R and S-R parts for the two energy-degenerate bright exciton states $|\uparrow_e, \downarrow_h, \mathbf{P}, \mathbf{K}\rangle$ and $|\downarrow_e, \uparrow_h, \mathbf{P}', \mathbf{K}'\rangle$. By referring to $|\uparrow_e, \downarrow_h, \mathbf{P}, \mathbf{K}\rangle$ and $|\downarrow_e, \uparrow_h, \mathbf{P}', \mathbf{K}'\rangle$ as “spin”-up $|\uparrow\rangle$ and “spin”-down $|\downarrow\rangle$ states, their matrix elements are denoted by $H_{\mathbf{K}-\mathbf{K}'}^{\text{A}} = \mathbf{\Omega}(\mathbf{P}) \cdot \mathbf{s}$ in the exciton “spin” space, with the effective magnetic field reading

$$\mathbf{\Omega}(\mathbf{P}) = \left(-C\alpha(1) \frac{P_x^2 - P_y^2}{|\mathbf{P}|} + \Xi, 2C\alpha(1) \frac{P_x P_y}{|\mathbf{P}|}, 0 \right). \quad (13)$$

Obviously, the L-R (S-R) part of the exchange interaction acts as an in-plane \mathbf{P} -dependent (static) magnetic field.

With the effective magnetic field, the inter-valley A-exciton dynamics can be described by the KSBEs:³⁴⁻³⁷

$$\partial_t \rho(\mathbf{P}, t) = \partial_t \rho(\mathbf{P}, t)|_{\text{coh}} + \partial_t \rho(\mathbf{P}, t)|_{\text{scat}}. \quad (14)$$

In these equations, $\rho(\mathbf{P}, t)$ represent the 2×2 density matrices of A-exciton with center-of-mass momentum \mathbf{P} at

time t , in which the diagonal elements $\rho_{s,s}(\mathbf{P}, t)$ describe the A-exciton distribution functions and the off-diagonal elements $\rho_{s,-s}(\mathbf{P}, t)$ represent the “spin” coherence. In the collinear space, the coherent term is given by

$$\partial_t \rho(\mathbf{P}, t)|_{\text{coh}} = -\frac{i}{\hbar} [\mathbf{\Omega}(\mathbf{P}) \cdot \mathbf{s}, \rho(\mathbf{P}, t)], \quad (15)$$

where $[\ , \]$ denotes the commutator. The scattering terms $\partial_t \rho(\mathbf{P}, t)|_{\text{scat}}$ include the inter-exciton scattering, exciton-phonon scattering and exciton-impurity scattering. Here, for simplicity, we only include the exciton-impurity scattering,³⁴ which is written as

$$\partial_t \rho(\mathbf{P}, t)|_{\text{scat}} = \sum_{\mathbf{P}'} W_{\mathbf{P}\mathbf{P}'} [\rho(\mathbf{P}', t) - \rho(\mathbf{P}, t)]. \quad (16)$$

Here, $W_{\mathbf{P}\mathbf{P}'}$ represents the momentum scattering rate.

By solving the KSBEs, one obtains the evolution of the valley polarization $P(t) = \sum_{\mathbf{P}} \text{Tr}[\rho(\mathbf{P}, t)s_z]/n_{ex}$ with $n_{ex} = \sum_{\mathbf{P}} \text{Tr}[\rho(\mathbf{P}, t)]$ being the density of the A-exciton. According to the pump-probe experiment,^{22,23} the initial condition is set to be

$$\rho_{s,s}(\mathbf{P}, 0) = \alpha_s \exp \left\{ -[\varepsilon(\mathbf{P}) - \varepsilon_{\text{pump}}]^2 / (2\delta_\varepsilon^2) \right\} \quad (17)$$

and $\rho_{s,-s}(\mathbf{P}, 0) = 0$. Here, $\varepsilon(\mathbf{P}) = \hbar^2 \mathbf{P}^2 / (2m^*)$ is the exciton kinetic energy with m^* being the exciton effective mass; $\varepsilon_{\text{pump}}$ is the energy of pulse center in reference to the band minimum and $\delta_\varepsilon = \hbar/\delta_\tau$ with δ_τ denoting the pulse width;

$$\alpha_s = \frac{n_{\text{pump},s}}{\sum_{\mathbf{P}} \exp \left\{ -[\varepsilon(\mathbf{P}) - \varepsilon_{\text{pump}}]^2 / (2\delta_\varepsilon^2) \right\}}, \quad (18)$$

with $n_{\text{pump},s}$ being the density of A-exciton with “spin” s after excitation. In the PL experiment or the pump-probe experiment, according to the chiral optical valley selection rule, we set $n_{\text{pump},\uparrow} = n_{\text{ex}}$ and $n_{\text{pump},\downarrow} = 0$.

2. Results

In this part, we look into the current valley polarization experiments in monolayer MoS₂ with A-exciton pumped: the time-resolved valley polarization measurement,²¹ the pump-probe experiment^{22,23} and the steady-state PL polarization measurement.^{5-8,18-20} Their theoretical explanations are summarized below based on the KSBEs [Eq. (14)]. The material parameters in our computation are listed in Table II.

TABLE II: Material parameters used in the computation.

| | | | |
|-------------------------------------|-------------------|--------------------------------|------------------|
| κ | 3.43 ^a | a_B (nm) | 2.0 ^c |
| m^*/m_0 | 0.28 ^b | τ_P^* (fs) | 6.0 |
| n_{ex} (cm ⁻²) | 10 ¹⁰ | $\alpha(1)$ (\AA^2) | 4.91 |

^a Ref. 11. ^b Refs. 28,42. ^c Refs. 40,43-45.

We first study the initial evolution of the valley polarization in the time-resolved polarization measurement in monolayer MoS₂ carried out by Lagarde *et al.*,²¹ in which the emergence of the A-exciton in the K' valley is almost immediate with the A-exciton pumped in the K valley. In the experiment, the pulse-center energy is away from the A-exciton resonance energy by $\varepsilon_{\text{pump}} \approx 100$ meV and the laser pulse width $\delta_t \approx 1.6$ ps.²¹ With this pulse, the center-of-mass momentum $|\mathbf{P}| = \sqrt{2m^*\varepsilon_{\text{pump}}}/\hbar$ of the A-exciton is large. From Eq. (13), the precession frequency due to the L-R exchange interaction between the two exciton “spin” states is estimated to be

$$\omega(\mathbf{P}) \approx \sqrt{5}C\alpha(1)|\mathbf{P}|/\hbar, \quad (19)$$

which is proportional to $|\mathbf{P}|$. Obviously, when $|\mathbf{P}|$ is large (small), the precession frequency between the two exciton “spin” states is large (small) and the L-R exchange interaction causes *fast* (*slow*) inter-valley exciton precession. Specifically, when $|\mathbf{P}| = 0$, the inter-exciton precession due to the L-R exchange interaction is forbidden and the inter-valley exciton precession time is expected to be very long. Accordingly, in the experiment of Lagarde *et al.*,²¹ due to the large initial A-exciton center-of-mass momentum, the inter-valley exciton precession time is estimated to be $T = \pi/\omega(\mathbf{P}) = 13$ fs, which is much shorter than the uncertainty of time origin, i.e., 700 fs in the experiment.²¹ Therefore, the observation of the excitonic signal in the K' valley is immediate after the A-exciton pumped in K valley in the experiment.²¹ Here, the S-R exchange interaction is not considered. Only the L-R exchange interaction can well explain the experiment.²¹ For the S-R exchange interaction, unlike the L-R component, so far there lacks the material parameter Ξ [Eq. (11)]. Furthermore, according to the experience in semiconductors, the S-R exchange interaction is much smaller than the L-R one.^{37,39,46} Therefore, the S-R exchange interaction is speculated to be negligible here.

We then investigate the dynamics of the valley polarization in the pump-probe experiments for monolayer MoS₂ based on the KSBs with the A-exciton resonantly pumped in the K valley.^{22,23} In our calculation, the momentum relaxation time τ_P^* in Table II is obtained based on the elastic scattering approximation as a first step in the investigation,³⁴ which can be varied by tuning $W_{\mathbf{P}\mathbf{P}'}$ [Eq. (16)] in the calculation. Its value is estimated to be 6 fs by considering the measured broadening of the A exciton energy $\Gamma \approx 110$ meV at 4 K with $\tau_P^* \approx \hbar/\Gamma$.^{21,48} By setting $\varepsilon_{\text{pump}} = 0$ eV and $\delta_t = 60$ fs according to Mai *et al.*,²² with the material parameters in Table II, the evolution of the valley polarization with different scattering strengths can be obtained by numerically solving the KSBEs, shown in Fig. 2.

From Fig. 2, several features of the dynamics of the valley polarization can be obtained, which are in good agreement with the experimental observations in the pump-probe set-up.^{22,23} It is observed that when the A-exciton is resonantly pumped in the K valley, even at the time overlap of the pump and probe pulses, there are exci-

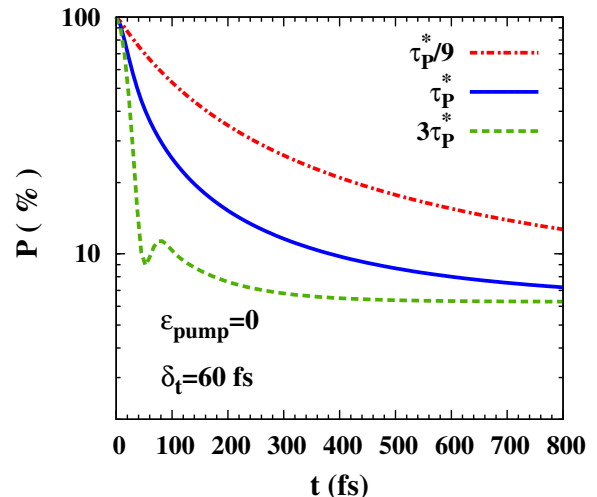


FIG. 2: (Color online) Evolution of the valley polarization when A-exciton is resonantly pumped in the K valley with different momentum relaxation times $\tau_P^*/9$, τ_P^* and $3\tau_P^*$, respectively. The pulse width is chosen to be $\delta_t = 60$ fs according to Ref. 22.

tonic signals of the A-exciton in the K' valley. Here, in our computation, it is shown that with the A-exciton resonantly pumped in the K valley, when the momentum scattering is relatively weak (the green dashed curve with momentum relaxation time $3\tau_P^*$), it takes only several femtoseconds for the transition of the A-exciton from the K valley to the K' valley; even the momentum scattering is relatively strong, this inter-valley transition time for the A-exciton is still in the order of tens of femtoseconds. This is also due to the large center-of-mass momentum of the exciton, the effective magnetic field due to the L-R exchange interaction can cause fast inter-exciton “spin” precession. Furthermore, it is also reported in the experiment²² that the polarization anisotropy in the A transition is completely lost in about 400 fs, which indicates the valley depolarization time is hundreds of femtoseconds. Our calculation also shows that no matter the momentum scattering is relative weak (the green dashed curve with momentum relaxation time $3\tau_P^*$) or strong (the red chain curve with momentum relaxation time $\tau_P^*/9$), the valley depolarization times are in the order of hundreds of femtoseconds. Moreover, in the experiment,²² it shows that the total valley polarization does not completely relax for about 10 ps, which hints the existence of the residue valley polarization which lasts for a very long time. In our computation, it is also observed that there are residue valley polarizations (about 10%) lasting for several picoseconds. This residue valley polarization originates from the small effective magnetic field due to the L-R exchange interaction with small $|\mathbf{P}|$ and hence long valley depolarization time, in contrast to the fast inter-exciton precession with large $|\mathbf{P}|$. Furthermore, due to the energy relaxation of the excitons, with the increase of the ratio of the excitons with small $|\mathbf{P}|$,

the residue valley polarization increases.

Finally, we address the series of steady-state measurements of the PL polarization.^{5,7,18-20} In these experiments, a wide range of residue valley polarizations from 30% to 100% are reported with the A-exciton resonantly pumped at low temperature.^{5,7,18-20} These steady-state residue PL polarizations can be estimated by the rate equations,^{5,18,19,21,47} a simplified KSBEs, with the valley depolarization time and exciton lifetime known. We point out that it has been addressed by us with the S-R exchange interaction only⁴⁷ and by Glazov *et al.* very recently with the L-R exchange interaction.⁴⁸ However, based on the above understanding, we conclude that the L-R exchange interaction should be more important than the S-R one in the valley depolarization.

III. CONCLUSION AND DISCUSSION

In conclusion, we have investigated the valley depolarization due to the e-h exchange interaction in monolayer MoS₂. Both the L-R and S-R parts of the exchange interactions for the inter- and intra-valley e-h interactions are calculated. We find that both the L-R and S-R exchange interactions can cause the inter- and intra-valley bright exciton transitions. However, the intra-valley bright exciton transition channel is nearly forbidden due to the large splitting of the valence bands. For the inter-valley bright exciton transition, we show that for the A-exciton with large center-of-mass momentum, the L-R exchange interaction can cause the *fast* inter-valley exciton transition. This explains the fast emergence of the excitonic signal in the K' valley with the A-exciton pumped in K valley in the experiments.²¹⁻²³ However, for the A-exciton with small center-of-mass momentum, the inter-valley exciton transition is relatively *slow* and this leads to the existence of the residue valley polarization which lasts for tens of picoseconds in the experiments.^{22,23} As for the S-R exchange interaction, whose strength is unavailable due to lack of the material parameter in the literature, it is speculated to be negligible. More investigations are needed to further clarify this problem.

Finally, we address other possible valley depolarization mechanisms in the literature. For the DP and EY mechanisms, only the extrinsic influences can cause the relaxation of the out-of-plane component of the electron/hole spin but with low efficiency, which cannot cause the inter-valley exciton transition effectively. Apart from the inter-valley exciton transition, there also exist other arguments for the possible cause of the valley depolarizations in the experiments. It was argued that the out-of-plane component of the hole spin can relax after scattering to the Γ valley through the DP or EY mechanisms.²² However, this is impossible as \hat{s}_z is also a good quantum number for the Γ valley, apart from the fact that there is no effective relaxation channel for the electron spin.^{28,29} In addition, tight-binding simulations show that the disordered defects can weaken the chiral optical valley selection rule

when the excitation is away from the vicinity of the high symmetry K(K') point.²³ However, only very strong disorder can significantly decrease the valley polarization,²³ which is unlikely in the clean samples.

Acknowledgments

This work was supported by the National Natural Science Foundation of China under Grant No. 11334014, the National Basic Research Program of China under Grant No. 2012CB922002 and the Strategic Priority Research Program of the Chinese Academy of Sciences under Grant No. XDB01000000. One of the authors (TY) would like to thank L. Wang for valuable discussions.

Appendix A: Exciton Hamiltonian

In this appendix, based on the lowest four band $\mathbf{k} \cdot \mathbf{p}$ Hamiltonian [Eq. (1)], we give the explicit form of the exciton Hamiltonian $H_{mn}^{\text{eh}}(\mathbf{r}'_1, \mathbf{r}'_2)$ for the direct exciton envelop function $F_{mn}(\mathbf{r}_1, \mathbf{r}_2)$ in the coordinate space, where $m(m')$ and $n(n')$ represent the band indexes in the K or K' valley labeled by the electron spin for the conduction band and hole spin for the valence band, respectively.^{34,38,39} The eigenequation expressed by the exciton Hamiltonian for the exciton envelop function satisfies

$$\sum_{mn} \int d\mathbf{r}_1 d\mathbf{r}_2 H_{mn}^{\text{eh}}(\mathbf{r}'_1, \mathbf{r}'_2) F_{mn}(\mathbf{r}_1, \mathbf{r}_2) = EF_{m'n'}(\mathbf{r}'_1, \mathbf{r}'_2), \quad (\text{A1})$$

where

$$\begin{aligned} H_{mn}^{\text{eh}}(\mathbf{r}'_1, \mathbf{r}'_2) &= [H_{m'm}^e(\mathbf{k}_1)\delta_{n'n} + H_{n'n}^h(\mathbf{k}_2)\delta_{m'm} \\ &+ U^{\text{eh}}(\mathbf{r}_1 - \mathbf{r}_2)\delta_{m'm}\delta_{n'n}]\delta(\mathbf{r}_1 - \mathbf{r}'_1)\delta(\mathbf{r}_2 - \mathbf{r}'_2) \\ &+ H_{mn}^{\text{ex}}(\mathbf{r}'_1, \mathbf{r}'_2). \end{aligned} \quad (\text{A2})$$

Here, $\mathbf{k} = -i\nabla$,

$$U^{\text{eh}}(\mathbf{r}_1 - \mathbf{r}_2) = -\frac{e^2}{4\pi\epsilon_0\kappa|\mathbf{r}_1 - \mathbf{r}_2|}, \quad (\text{A3})$$

$$\begin{aligned} &H_{m'm}^e(\mathbf{k}_1) \\ &= E_m(\mathbf{k}_0) + \frac{\hbar^2}{2m_0^2} \sum_{m''} [\mathbf{k}_1 \cdot \boldsymbol{\pi}_{m'm''}(\mathbf{k}_0)] [\mathbf{k}_1 \cdot \boldsymbol{\pi}_{m''m}(\mathbf{k}_0)] \\ &\times \left[\frac{1}{E_m(\mathbf{k}_0) - E_{m''}(\mathbf{k}_0)} + \frac{1}{E_{m'}(\mathbf{k}_0) - E_{m''}(\mathbf{k}_0)} \right], \end{aligned} \quad (\text{A4})$$

and

$$H_{n'n}^h(\mathbf{k}_2) = -H_{\Theta n \Theta n'}^e(-\mathbf{k}_2), \quad (\text{A5})$$

We have $\boldsymbol{\pi} = \mathbf{p} + \frac{\hbar}{4m_0^2c^2}[\boldsymbol{\sigma} \times (\nabla V_0)]$ with V_0 denoting the lattice potential. $\boldsymbol{\pi}_{ss'}(\mathbf{k}_0)$ stands for the matrix elements of $\boldsymbol{\pi}$ between two Bloch wavefunctions in the s and s' bands (s and s' are electron spins). The nonzero expressions of $\boldsymbol{\pi}_{ss'}(\mathbf{k}_0)$ in the K or K' valley can be obtained from the Hamiltonian Eq. (1). For the K ($\tau = 1$) or K' ($\tau = -1$) valley,

$$\langle \uparrow_c | \pi_x | \downarrow_h \rangle = \langle \downarrow_c | \pi_x | \uparrow_h \rangle = \tau m_0 a t / \hbar \quad (\text{A6})$$

and

$$\langle \uparrow_c | \pi_y | \downarrow_h \rangle = \langle \downarrow_c | \pi_y | \uparrow_h \rangle = -i m_0 a t / \hbar. \quad (\text{A7})$$

The electron-hole exchange interaction Hamiltonian is divided into L-R and S-R parts:

$$H_{mn}^{\text{ex}} \left(\begin{array}{c} \mathbf{r}'_1 \ \mathbf{r}'_2 \\ \mathbf{r}_1 \ \mathbf{r}_2 \end{array} \right) = H_{mn}^{\text{LR}} \left(\begin{array}{c} \mathbf{r}'_1 \ \mathbf{r}'_2 \\ \mathbf{r}_1 \ \mathbf{r}_2 \end{array} \right) + H_{mn}^{\text{SR}} \left(\begin{array}{c} \mathbf{r}'_1 \ \mathbf{r}'_2 \\ \mathbf{r}_1 \ \mathbf{r}_2 \end{array} \right). \quad (\text{A8})$$

For the L-R exchange interaction,

$$\begin{aligned} & H_{mn}^{\text{LR}} \left(\begin{array}{c} \mathbf{r}'_1 \ \mathbf{r}'_2 \\ \mathbf{r}_1 \ \mathbf{r}_2 \end{array} \right) \\ &= - \sum_{\alpha\beta} Q_{\frac{m'\Theta_n}{\Theta_n'm}}^{\mathbf{k}_0-\mathbf{k}'_0} \Big|_{\alpha\beta} \frac{\partial^2}{\partial \mathbf{r}_1^\alpha \partial \mathbf{r}_1^\beta} U(\mathbf{r}_1 - \mathbf{r}'_2) \delta(\mathbf{r}_1 - \mathbf{r}_2) \delta(\mathbf{r}'_1 - \mathbf{r}'_2), \end{aligned} \quad (\text{A9})$$

with

$$\begin{aligned} Q_{\frac{m'\Theta_n}{\Theta_n'm}}^{\mathbf{k}_0-\mathbf{k}'_0} \Big|_{\alpha\beta} &= \frac{\hbar^2}{m_0^2} \pi_{m'\Theta_n'}^\alpha(\mathbf{k}_0) \pi_{\Theta_n m}^\beta(\mathbf{k}'_0) \\ &\times \frac{1}{[E_m(\mathbf{k}_0) - E_n(\mathbf{k}_0)][E_{m'}(\mathbf{k}'_0) - E_{n'}(\mathbf{k}'_0)]} \end{aligned} \quad (\text{A10})$$

and α (β) denoting x or y . For the S-R exchange interaction,

$$H_{mn}^{\text{SR}} \left(\begin{array}{c} \mathbf{r}'_1 \ \mathbf{r}'_2 \\ \mathbf{r}_1 \ \mathbf{r}_2 \end{array} \right) = S U_{\frac{m'\Theta_n}{\Theta_n'm}} \delta(\mathbf{r}_1 - \mathbf{r}_2) \delta(\mathbf{r}_1 - \mathbf{r}'_1) \delta(\mathbf{r}_2 - \mathbf{r}'_2), \quad (\text{A11})$$

with

$$\begin{aligned} U_{\frac{m'\Theta_n}{\Theta_n'm}} &= \frac{1}{S^2} \int d\mathbf{r}_1 d\mathbf{r}_2 [\Psi_{\mathbf{k}'_0}^{m'}(\mathbf{r}_1)]^* [\Theta \tilde{\Psi}_{\mathbf{k}_0}^n(\mathbf{r}_2)]^* \\ &\times U(\mathbf{r}_1 - \mathbf{r}_2) [\Theta \tilde{\Psi}_{\mathbf{k}'_0}^{n'}(\mathbf{r}_1)] \Psi_{\mathbf{k}_0}^m(\mathbf{r}_2). \end{aligned} \quad (\text{A12})$$

-
- * Author to whom correspondence should be addressed; Electronic address: mwwu@ustc.edu.cn.
- 1 B. Radisavljevic, A. Radenovic, J. Brivio, V. Giacometti, and A. Kis, *Nature Nanotech.* **6**, 147 (2011).
 - 2 Y. Yoon, K. Ganapathi, and S. Salahuddin, *Nano Lett.* **11**, 3768 (2011).
 - 3 H. Liu and P. D. Ye, *IEEE Electron Dev. Lett.* **33**, 546 (2012).
 - 4 W. Yao, D. Xiao, and Q. Niu, *Phys. Rev. B* **77**, 235406 (2008).
 - 5 T. Cao, G. Wang, W. Han, H. Ye, C. Zhu, J. Shi, Q. Niu, P. Tan, E. Wang, B. Liu, and J. Feng, *Nature Commun.* **3**, 887 (2012).
 - 6 D. Xiao, G. B. Liu, W. Feng, X. Xu, and W. Yao, *Phys. Rev. Lett.* **108**, 196802 (2012).
 - 7 G. Sallen, L. Bouet, X. Marie, G. Wang, C. R. Zhu, W. P. Han, Y. Lu, P. H. Tan, T. Amand, B. L. Liu, and B. Urbaszek, *Phys. Rev. B* **86**, 081301(R) (2012).
 - 8 A. Splendiani, L. Sun, Y. Zhang, T. Li, J. Kim, C. Y. Chim, G. Galli, and F. Wang, *Nano Lett.* **10**, 1271 (2010).
 - 9 Z. Y. Zhu, Y. C. Cheng, and U. Schwingenschlöggl, *Phys. Rev. B* **84**, 153402 (2011).
 - 10 K. Kaasbjerg, K. S. Thygesen, and K. W. Jacobsen, *Phys. Rev. B* **85**, 115317 (2012).
 - 11 T. Cheiwchanhanngij and W. R. L. Lambrecht, *Phys. Rev. B* **85**, 205302 (2012).
 - 12 H. Shi, H. Pan, Y. W. Zhang, and B. I. Yakobson, *Phys. Rev. B* **87**, 155304 (2013).
 - 13 X. Li, J. T. Mullen, Z. Jin, K. M. Borysenko, M. B.

- Nardelli, and K. W. Kim, *Phys. Rev. B* **87**, 115418 (2013).
- 14 E. S. Kadantsev and P. Hawrylak, *Solid State Commun.* **152**, 909 (2012).
- 15 K. Kořmider and J. F. Rossier, *Phys. Rev. B* **87**, 075451 (2013).
- 16 H. Ochoa and R. Roldán, *Phys. Rev. B* **87**, 245421 (2013).
- 17 F. Zahid, L. Liu, Y. Zhu, J. Wang, and H. Guo, *AIP Advances* **3**, 052111 (2013).
- 18 K. F. Mak, K. He, J. Sahn, and T. F. Heinz, *Nature Nanotech.* **7**, 494 (2012).
- 19 G. Kioseoglou, A. T. Hanbicki, M. Currie, A. L. Friedman, D. Gunlycke, and B. T. Jonker, *Appl. Phys. Lett.* **101**, 221907 (2012).
- 20 H. Zeng, J. Dai, W. Yao, D. Xiao, and X. Cui, *Nature Nanotech.* **7**, 490 (2012).
- 21 D. Lagarde, L. Bouet, X. Marie, C. R. Zhu, B. L. Liu, T. Amand, and B. Urbaszek, *Phys. Rev. Lett.* **112**, 047401 (2014).
- 22 C. Mai, A. Barrette, Y. Yu, Y. G. Semenov, K. W. Kim, L. Cao, and K. Gundogdu, *Nano Lett.* **14**, 202 (2014).
- 23 Q. Wang, S. Ge, X. Li, J. Qiu, Y. Ji, J. Feng, and D. Sun, *ACS Nano* **7**, 11087 (2013).
- 24 M. I. D'yakonov and V. I. Perel', *Zh. Eksp. Teor. Fiz.* **60**, 1954 (1971) [*Sov. Phys. JETP* **33**, 1053 (1971)].
- 25 Y. Yafet, *Phys. Rev.* **85**, 478 (1952).
- 26 R. J. Elliott, *Phys. Rev.* **96**, 266 (1954).
- 27 L. Wang and M. W. Wu, *Phys. Lett. A*, 2014, in press; arXiv:1305.3361v2.
- 28 A. Kormányos, V. Zólyomi, N. D. Drummond, P. Rakyta,

- G. Burkard, and V. I. Fal'ko, Phys. Rev. B **88**, 045416 (2013).
- ²⁹ H. Rostami, A. G. Moghaddam, and R. Asgari, Phys. Rev. B **88**, 085440 (2013).
- ³⁰ H. Ochoa and R. Roldán, Phys. Rev. B **87**, 245421 (2013).
- ³¹ H. Ochoa, F. Guinea, and V. I. Fal'ko, Phys. Rev. B **88**, 195417 (2013).
- ³² L. Wang and M. W. Wu, Phys. Rev. B **89**, 115302 (2014).
- ³³ T. Korn, S. Heydrich, M. Hirmer, J. Schmutzler, and C. Schüller, Appl. Phys. Lett. **99**, 102109 (2011).
- ³⁴ M. Z. Maialle, E. A. de Andrada e Silva, and L. J. Sham, Phys. Rev. B **47**, 15776 (1993).
- ³⁵ A. Vinattieri, Jagdeep Shah, T. C. Damen, D. S. Kim, L. N. Pfeiffer, M. Z. Maialle, and L. J. Sham, Phys. Rev. B **50**, 10868 (1994).
- ³⁶ M. W. Wu and C. Z. Ning, Eur. Phys. J. B. **18**, 373 (2000); M. W. Wu, J. Phys. Soc. Jpn. **70**, 2195 (2001).
- ³⁷ M. W. Wu, J. H. Jiang, and M. Q. Weng, Phys. Rep. **493**, 61 (2010).
- ³⁸ G. E. Pikus and G. L. Bir, Zh. Eksp. Teor. Fiz. **60**, 195 (1971) [Sov. Phys. JETP **33**, 108 (1973)].
- ³⁹ H. Tong and M. W. Wu, Phys. Rev. B **83**, 235323 (2011).
- ⁴⁰ A. Ramasubramaniam, Phys. Rev. B **86**, 115409 (2012).
- ⁴¹ H. Haug and A.-P. Jauho, *Quantum Kinetics in Transport and Optics of Semiconductors* (Springer-Verlag, Berlin, 1996).
- ⁴² K. Kaasbjerg, K. S. Thygesen, and K. W. Jacobsen, Phys. Rev. B **85**, 115317 (2012).
- ⁴³ T. Cheiwchanamngij and W. R. L. Lambrecht, Phys. Rev. B **85**, 205302 (2012).
- ⁴⁴ F. J. Crowne, M. Amani, A. G. Birdwell, M. L. Chin, T. P. O'Regan, S. Najmaei, Z. Liu, P. M. Ajayan, J. Lou, and M. Dubey, Phys. Rev. B **88**, 235302 (2013).
- ⁴⁵ C. Zhang, H. Wang, W. Chan, C. Manolaton, and F. Rana, arXiv:1402.0263.
- ⁴⁶ *Numerical Data and Functional Relationships in Science and Technology*, Landolt-Börnstein, New Series, Group III, Vol. 17, Pt. A, edited by O. Madelung, M. Schultz, and H. Weiss (Springer-Verlag, Berlin, 1982).
- ⁴⁷ T. Yu and M. W. Wu, arXiv:1401.0047v2.
- ⁴⁸ M. M. Glazov, T. Amand, X. Marie, D. Lagarde, L. Bouet, and B. Urbaszek, arXiv:1403.0108.